Heterogeneity of colloidal particle networks analyzed by means of Minkowski functionals

Markus Hütter*
ETH-Zurich, Department of Materials, Institute of Polymers, CH-8092 Zurich, Switzerland
(Received 20 December 2002; revised manuscript received 30 June 2003; published 12 September 2003)

The heterogeneity and large scale connectivity of colloidal particle networks, which are generated by Brownian dynamics simulations, is examined. This is achieved by employing integral geometric measures in the form of the Minkowski functionals or quermassintegrals. It is found that these measures in conjunction with the parallel-body technique amount to a powerful tool to characterize the structure, going beyond the information contained in the pair-correlation function. The development of heterogeneities during network formation as well as their dependence on the volume fraction and the interaction potential is studied. In particular, it is found that slow coagulation enhances the heterogeneity of the network compared to fast coagulation.

DOI: 10.1103/PhysRevE.68.031404 PACS number(s): 82.70.Gg, 02.40.−k, 61.43.−j

I. INTRODUCTION

Colloidal systems experience significant attention not only from experimentalists but also from theoreticians, as they may serve as model systems for atomic systems. Due to their characteristic length and time scales, interesting phenomena become experimentally accessible. Such phenomena include complex flow behavior such as shear thinning and shear thickening, as well as the formation of flocs, aggregates, and gels upon destabilization. In the following, we focus our attention on the characterization of the structure of colloidal gels, in particular, on finding reasonable means beyond the pair-correlation function to describe the structure.

In experiments at low volume fractions, the structure characterization of colloidal particle aggregates is often performed by transmission electron microscope (TEM) [1–3] or by scattering techniques [4,5], where the latter directly results in the pair-correlation function $g(r)$ for dilute systems. In nondilute systems, light scattering includes contributions from multiple scattering which need to be eliminated by either using cross-correlation techniques [6–9], index matching [10], or small angle neutron scattering [11]. Contrary, the concept of porosity and pore size distribution used for the characterization of rigid bodies and compacted powders [12,13] captures aspects clearly beyond the capability of pair-correlation functions, e.g., connectedness, and thus provides useful additional information [13]. In nonrigid materials, the determination of the porosity is a formidable task. Freeze-fracture techniques in combination with TEM [14,15] or cryogenic scanning electron microscope (cryo-SEM) [15,16] have been used to study the microstructure of concentrated suspensions. To hinder the formation of large ice crystals [17], cryo-SEM in connection with high-pressure freezing [18] has recently been applied to examine the structure of surface sections [19]. In order not to be restricted to the analysis of surface sections, restricted diffusion in freeze-dried food has been studied using nuclear magnetic resonance techniques, which allows to get a certain measure of the pore size distribution of the network as well [20]. However, most detailed local structural and dynamical information in dense systems has recently been obtained with confocal laser scanning microscopy. This direct visualization technique has been used to study colloidal gels and glasses [21–24] via time-resolved determination of the particles' three-dimensional (3D) coordinates. Nevertheless, irrespective of the problems encountered in the experimental structure characterization, the following question remains still open. If one aims at establishing a relation between the structure of the particle gel and macroscopic, e.g., mechanical properties, it is unresolved which measures of the network structure capture those features relevant for understanding the macroscopic properties. It is noteworthy that even if all particle coordinates would be known, e.g., as in the case of Brownian dynamics simulation studies [25–32] or confocal laser scanning microscopy [21–24], the relation between gel structure and mechanical properties remains obscured due to the vast amount of information on the particulate level. Thus, bridging the gap from the particle to the network scale and understanding their inter-relation means to introduce an intermediate level of coarse graining. In order to gain a better understanding of the structure-property relationship, it is of paramount importance to discuss the proper choice of coarse-grained measures of the particle gel structure. Considering the concept of the so-called load-bearing strings or force chains in granular media [33–36], we can anticipate that also in colloidal networks such substructures are relevant, which are not described by the pair-correlation function.

Computer simulations, and, in particular, Brownian dynamics simulations, are in the mean time well recognized as being appropriate for studying colloidal systems, and have been used extensively in recent years also to study the coagulation behavior and network formation (see, e.g., Refs. [25–32]). Concerning the network structure characterization, most of this work is restricted to give information on the pair-distribution function $g(r)$, either directly or by means of the mass-fractal dimension. Only little information is available beyond $g(r)$, e.g., in the form of bond-angle distribution functions (depending on the three-point correlation function) [32] or in terms of the coordination number, which is restricted to provide short range information [29]. Only re-

*Present address: Department of Chemical Engineering, Massachusetts Institute of Technology, Cambridge, MA 02139, USA. FAX: +1 617 258-0546; Electronic address: mhuetter@mit.edu

cently, other measures closely related to the pore size distribution have been used to characterize the structure of the network, which have been found to clearly distinguish between simulated gels of differing texture [30,31].

Mathematics provides various tools to characterize geometrical objects. Whereas differential geometry is well known for the discussion of local properties for a given surface, e.g., critical and saddle points, it is the main focus of integral geometry to find measures for the overall morphology and topology of the structure, i.e., also for the connectivity. We here want to illustrate to what extent the integral geometric measures, which crystallize into the so-called Minkowski functionals and the parallel-body technique, are useful to examine colloidal particle networks. For that purpose we analyze particle networks generated by our Brownian dynamics simulation scheme used in previous studies [32,37].

The paper is organized a follows. After introducing the Minkowski functionals in the following section and establishing their link to the pore size distribution used in Refs. [30,31], they are then used to analyze configurations generated by Brownian dynamics simulations of coagulating colloidal systems for different volume fractions and interaction potentials.

II. CHARACTERIZATION OF PARTICLE-NETWORK STRUCTURES

A. Minkowski functionals

We here give a short introduction to the Minkowski functionals of integral geometry. For more details the reader is referred to Refs. [38–41]. Minkowski functionals, also known as intrinsic volumes (quermassintegrals, curvature integrals), are used in integral geometry to characterize surfaces and shapes. If A denotes a compact domain in $\mathbb{R}^d$ with regular boundary $\partial A \in \mathcal{C}^2$, and $d-1$ principal radii of curvature R_i $(i=1,\ldots,d-1)$, functionals W_ν $(\nu \geqslant 1)$ can be defined by the following surface integrals:

$$W_{\nu+1}(A) = \frac{1}{(\nu+1)\binom{d}{\nu+1}} \int_{\partial A} S_\nu\left(\frac{1}{R_1},\ldots,\frac{1}{R_{d-1}}\right) d\mathcal{S}, \tag{1}$$

where S_ν is the νth elementary symmetric function and $d\mathcal{S}$ denotes the $(d-1)$-dimensional surface element. In the specific situation of a two-dimensional surface embedded in three-dimensional space, we find

$$W_1 = \frac{1}{3}\int_{\partial A} d\mathcal{S}, \quad W_2 = \frac{1}{3}\int_{\partial A} \frac{1}{2}\left(\frac{1}{R_1}+\frac{1}{R_2}\right) d\mathcal{S},$$

$$W_3 = \frac{1}{3}\int_{\partial A} \frac{1}{R_1 R_2} d\mathcal{S}. \tag{2}$$

Note that the integrand in W_2 is the mean curvature, whereas the integrand in W_3 is the Gaussian curvature (usually denoted by H and G, respectively). Although using the concept of regular surfaces for their definition here, the Minkowski functionals are also well defined for polyhedra with singular edges [39]. In addition to the above definitions in terms of surface integrals, the zeroth Minkowski functional W_0 is defined as the volume of the compact domain A. Conclusively, the functional W_ν has dimension $(\text{length})^{d-\nu}$ $(\nu = 0,1,\ldots,d)$. As an example, for a set of N nonoverlapping spheres of radius R in $\mathbb{R}^3$, the values of the functionals are

$$W_\nu = N\frac{4\pi}{3}R^{3-\nu} \quad (\nu = 0,1,2,3). \tag{3}$$

In general, the characterization of a domain $A \subset \mathbb{R}^3$ as described above results in four numbers, $W_\nu(A)$ $(\nu = 0,1,2,3)$, measuring (i) volume, (ii) surface, (iii) average mean curvature (a characteristic length scale), and (iv) the connectivity. The latter is defined as the number of disconnected components plus the number of cavities minus the number of tunnels of the domain A, i.e., it is a topological measure. It will prove to be of substantial interest in the study of colloidal gels. The understanding of the morphology and topology of a domain A can be substantially enhanced by examining the functionals when ''blowing up'' the domain A. More rigorously speaking, one can study the Minkowski functionals of the ε surrounding $(\varepsilon \geqslant 0)$ of A, $A_\varepsilon := \{\mathbf{y} \,|\, \|\mathbf{y}-\mathbf{x}\| \leqslant \varepsilon, \mathbf{x} \in A\}$. The domain A_ε is then called a parallel body of A. The study of the Minkowski functionals $W_\nu(A_\varepsilon)$, which are now functions of ε [in contrast to $W_\nu(A)$], allows for a deeper understanding of the structure, as shall be illustrated in this paper. The parallel-body technique is particularly useful when analyzing the structure of a many-particle system of equally sized spheres with radius R, e.g., colloidal particle gels. Consider a set of N spheres in domain Ω, with the n-point distribution functions $\rho_n(\Gamma_n)$ $(n=1,\ldots,N)$ with $\Gamma_n \equiv (\mathbf{x}_1,\ldots,\mathbf{x}_n)$ and let $A_r = \cup_{i=1}^N B_r(\mathbf{x}_i)$, where $B_r(\mathbf{x}_i)$ is a sphere of radius r and center $\mathbf{x}_i$. Our interest is now in the properties of the surface of this union of penetrable spheres, ∂A_r. It can be shown that the Minkowski functionals for A_r are given by (see, e.g., Ref. [42])

$$W_\nu(A_r;\{\rho_n\}) = \sum_{n=1}^{N} \frac{(-1)^{n+1}}{n!} \int_\Omega d\Gamma_n W_\nu\left(\bigcap_{i=1}^{n} B_r(\mathbf{x}_i)\right) \times \rho_n(\Gamma_n) \quad (\nu = 0,1,2,3). \tag{4}$$

For $r=R$, we recover the four values for the Minkowski functionals of the real structure. Note that the Minkowski functionals capture some information of all n-point distribution functions in a condensed form due to the overlapping of n (imaginary) spheres. However, this information can only be recovered through the r dependence of the four functions given in Eq. (4). This fact raises the hope that, by using functionals (4), information can be revealed which is not accessible through the pair-correlation function commonly employed. In the present study we attempt to illustrate to what extent the parallel-body technique in conjunction with the Minkowski functionals offers a useful tool for characterizing the structure, in particular, also the heterogeneity, of the colloidal particle networks. This technique has been successfully applied for analyzing the structure of a Lennard-Jones

TABLE I. Potential parameters for the coagulating suspension.

Parameter	Symbol	Value	Units (SI)
Hamaker constant of Al_2O_3 in water	A_H	4.76×10^{-20}	J
Particle radius	$R=d/2$	2.5×10^{-7}	m
Relative dielectric constant of water	ϵ_r	81	
Absolute temperature	T	293	K
Valency of ions	z	1	
Surface potential	ψ_0	0.0–0.015	V
Inverse Debye screening length	κ	10^{+8}	m^{-1}

fluid [42] and in cosmology for quantifying higher-order correlations of galaxy cluster distributions [43,44].

B. A possible definition of "pore size distribution"

We here briefly address a possible definition of ''pores'' in a network and the corresponding pore size distribution. In particulate networks, this question is interesting since, e.g., two pores connected by a tunnel could also be considered one pore, depending on ratio of the tunnel diameter to the diameter of the ''big'' pores. Thus, counting pores is in principle a highly nontrivial problem, at least in particulate networks. Among other structure characterization methods, the following definition of the pore size distribution is discussed in Refs. [45–47]: It is given by the normalized probability $p(r')dr'$ that a randomly placed point lies in the interval $[r',r'+dr'[$ from the surface of the closest particle, i.e., from the pore surface. It is straightforward to show that this distribution function $p(r')$ is proportional to the surface of the set A_r of (overlapping) spheres defined above with $r=R+r'$, i.e.,

$$p(r')=\mathcal{N}W_1(A_{R+r'};\{\rho_n\}), \tag{5}$$

where $\mathcal{N}$ is a normalization constant. We mention that this definition, which gives a useful measure for the pore size distribution, is distinct from the pore size distribution determined from mercury porosimetry for two reasons. First, in the latter method big pores with only small necks are counted as small pores of the size of the necks [12] and second, the former method overestimates the number of small pores since within every large pore a lot of test points are placed, also such close to the pore surface. Nevertheless, taking the stand point that integral geometric measures may be useful for the network characterization and also appeal due to their solid mathematical background, the pore size distribution defined above nicely fits into this concept. As the above definition of the pore size distribution function has been used in Refs. [30,31] to analyze colloidal particle gels, we attempt to show in this paper to what extent the use of *all four* Minkowski functionals is beneficial.

III. BROWNIAN DYNAMICS SIMULATIONS

A. Algorithm for particle dynamics

The general procedure for simulating the formation of the colloidal particle network used here has been described in detail in Refs. [32,37]. Particle motions are monitored in terms of solving N coupled stochastic differential equations for the three-dimensional position vectors $\mathbf{r}_i$ in the overdamped limit,

$$d\mathbf{r}_i=\frac{1}{\zeta}\mathbf{F}_i^{\mathrm{pot}}(\mathbf{r}_1,\ldots,\mathbf{r}_N)dt+\sqrt{2k_BT/\zeta}d\mathbf{W}_i \quad (i=1,\ldots,N), \tag{6}$$

in the absence of external forces and flow. In the present study, the system size is $N=8000$. The dissipative nature of the above equations originates from considering Stokes' drag with a friction coefficient ζ ($\zeta=6\pi\eta_{\mathrm{solvent}}R$ with $\eta_{\mathrm{solvent}}=10^{-3}$ Pa s), however, multiparticle hydrodynamic interactions are neglected. For the potential interaction forces $\mathbf{F}_i^{\mathrm{pot}}$ pairwise additivity of Derjaguin-Landau-Verwey-Overbeek-(DLVO) interaction forces is assumed, the latter consisting of van der Waals attraction and electrostatic double layer repulsion,

$$V^{\mathrm{pot}}=V^{\mathrm{vdW}}+V^{\mathrm{el}}, \tag{7}$$

with

$$V^{\mathrm{vdW}}(r)=\frac{-A_H}{12}\left[\frac{d^2}{r^2-d^2}+\frac{d^2}{r^2}+2\ln\left(\frac{r^2-d^2}{d^2}\right)\right], \tag{8}$$

$$V^{\mathrm{el}}(r)=\pi\epsilon_r\epsilon_0 d\left[\frac{4k_BT}{ze}\tanh\left(\frac{ze\psi_0}{4k_BT}\right)\right]^2\exp(-\kappa\{r-d\}). \tag{9}$$

The parameters used in this study are specified in Table I, and the resulting potential is displayed in Fig. 1. The corresponding values of the energy barrier ΔE, which denotes the barrier between the local maximum and the secondary minimum, is given in Table II.

The second term in the evolution equation (6) represents the influence of the Brownian forces, the amplitude of which is coupled to the friction coefficient in the first, damping term in Eq. (6) through the fluctuation-dissipation theorem of the second kind (see, e.g., Refs. [48,49]). A rigorous treatment of random forces is given within the stochastic calculus of the independent Wiener processes $\mathbf{W}_i$ [49,50]. The dynamic equations (6) have been solved using a two-step integration scheme with an order of weak convergence of 2 and an integration time step $\Delta t=10^{-6}$ s$\simeq(2\times10^{-5})\tau_{\mathrm{Br}}$ in comparison to the characteristic Brownian diffusion time τ_{Br}.

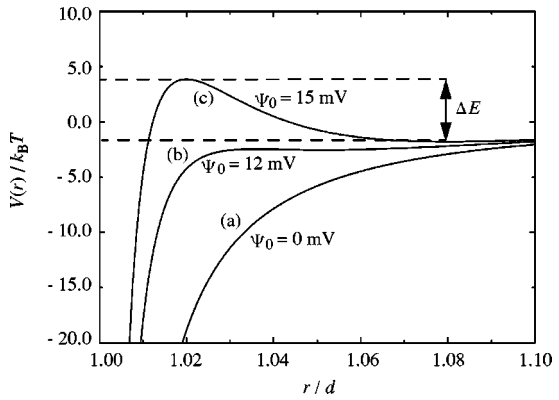

FIG. 1. DLVO-interaction potential $V(r/d)$ vs reduced center-to-center particle separation r/d (d particle diameter) for different surface potentials, and corresponding energy barrier ΔE: (a) pure van der Waals attraction, (b) $\Delta E/k_BT=0$, (c) $\Delta E/k_BT\simeq 5.65$.

For the implementation of the constraint motions of bonded particles, the reader is referred to Refs. [32,37].

B. Calculation method for Minkowski functionals

The Minkowski functionals $W_\nu(A_r;\{\rho_n\})$ for a point set given in Eq. (4) are calculated as follows. While the volume, $\nu=0$, is determined by Monte Carlo integration, one proceeds differently for $\nu=1,2,3$ as described in detail in Ref. [43]. The surface of the set A_r introduced in Sec. II A consists of piecewise spherical contours with curvature radius r. If two spheres intersect, these contours are joined along circular arcs, whereas there are singular points (vertices) if three spheres intersect. In the present study in the absence of regular crystalline arrangements, singular points where four or more spheres intersect have negligible weight and can therefore be neglected.

Consider now a sphere $B_r(\mathbf{x}_i)$ which is only partially covered by other spheres. If the amount of the uncovered area ∂B_i is denoted by S_i, the Minkowski functionals for $\nu=1,2,3$ for that particular surface become

$$W_{1,i}=\frac{1}{3}S_i, \quad W_{2,i}=\frac{1}{3r}S_i, \quad W_{3,i}=\frac{1}{3r^2}S_i. \tag{10}$$

On the intersection $B_r(\mathbf{x}_i)\cap B_r(\mathbf{x}_j)$ of two spheres, the uncovered arc A_{ij} of length l_{ij} results in the contributions

$$W_{2,ij}=\frac{1}{6}\alpha_{ij}l_{ij}, \quad W_{3,ij}=\frac{a_{ij}l_{ij}}{3r\sqrt{r^2-(a_{ij}/2)^2}}, \tag{11}$$

TABLE II. Energy barrier ΔE as a function of surface potential ψ_0.

ψ_0 (mV)	0.0–11.5	12.0	12.5	13.0	13.5	14.0	14.5	15.0
ΔE (k_BT)	0.0	0.076	0.522	1.20	2.07	3.01	4.31	5.65

with the angle α_{ij} between the normals of $B_r(\mathbf{x}_i)$ and $B_r(\mathbf{x}_j)$ along A_{ij}, and $\|\mathbf{x}_i-\mathbf{x}_j\|=a_{ij}<2r$. An uncovered vertex P_{ijk} at the common intersection of three spheres $B_r(\mathbf{x}_i)$, $B_r(\mathbf{x}_j)$, and $B_r(\mathbf{x}_k)$ contributes to W_3 through the solid angle spanned by the three surface normals at that position. Using l'Huilier's formula one finds

$$\left[\tan\left(\frac{3}{4}W_{3,ijk}\right)\right]^2 = \tan\left(\frac{\alpha_1+\alpha_2+\alpha_3}{4}\right)\tan\left(\frac{\alpha_1+\alpha_2-\alpha_3}{4}\right) \times\tan\left(\frac{\alpha_1-\alpha_2+\alpha_3}{4}\right)\tan\left(\frac{-\alpha_1+\alpha_2+\alpha_3}{4}\right), \tag{12}$$

with

$$\sin\left(\frac{\alpha_1}{2}\right)=\frac{\|\mathbf{x}_i-\mathbf{x}_j\|}{2r}, \quad \sin\left(\frac{\alpha_2}{2}\right)=\frac{\|\mathbf{x}_i-\mathbf{x}_k\|}{2r}, \quad \sin\left(\frac{\alpha_3}{2}\right)=\frac{\|\mathbf{x}_j-\mathbf{x}_k\|}{2r}. \tag{13}$$

In conclusion, the values for the functionals $W_\nu(A_r;\{\rho_n\})$ for $\nu=1,2,3$ become

$$W_1(A_r;\{\rho_n\})=\sum_i W_{1,i}, \tag{14}$$

$$W_2(A_r;\{\rho_n\})=\sum_i W_{2,i}-\sum_{ij} W_{2,ij}, \tag{15}$$

$$W_3(A_r;\{\rho_n\})=\sum_i W_{3,i}-\sum_{ij} W_{3,ij}+\sum_{ijk} W_{3,ijk}, \tag{16}$$

where the sums run over all uncovered surface pieces, arcs, and vertices. A description of how to deal with the particles intersecting the boundaries of the simulation box can be found in Ref. [51], and shall not be discussed here in more detail.

C. Simulations of network formation

1. Progressing network formation

The evaluation of the formation of colloidal particle gels is examined in the following. Here, as discussed above, this shall be achieved through studying the r dependence of the four Minkowski functionals $W_\nu(A_r;\{\rho_n\})$ ($\nu=0,1,2,3$) given in Eq. (4). In order to get an understanding of how characteristic features emerge in these four functions, we first study a progressing network formation of a sample at volume fraction $\phi=0.40$ and surface potential $\psi_0=0.0$ mV. The evolving network is built from particles in the primary minimum of the DLVO-interaction potential at particle surface contact, such bonds being considered irreversible. The states at the different stages are labeled by π_b

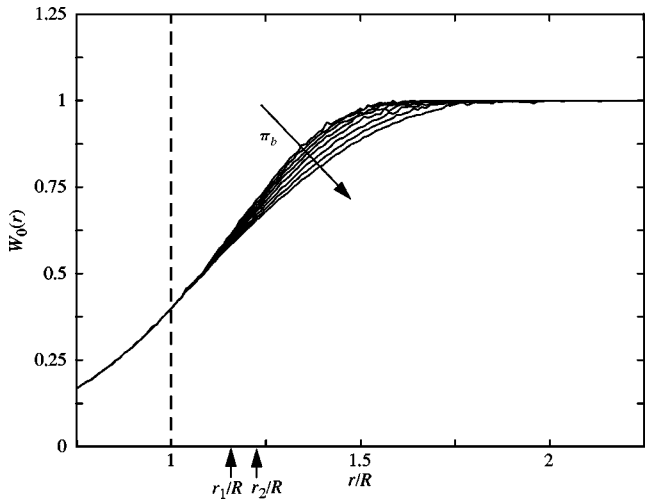

FIG. 2. Minkowski functional $W_0(r)$: Monitoring the progress of network formation of a sample with $\phi=0.4$ and $\Delta E/k_BT=0.0$.

which is defined as the number of bonded neighbors of each particle averaged over all particles (which would be in the range between 0 and 12 for spherical particles), and finally normalized by 12 (i.e., $0\leqslant\pi_b\leqslant 1$, $\pi_b=1$ only for hexagonal close packing). The Minkowski functionals for the different values of π_b are shown in Figs. 2–5, where the arrows point in the direction of progressing network formation. The r values are normalized with respect to the (real) particle radius R. As the values of (W_1,W_2,W_3) overall scale with the number of particles, these functions have been normalized with respect to their values of the real system at $r=R$. (For example, the volume fraction is restricted to $[0,1]$, whereas the amount of interface per volume can in principle become arbitrarily large.) Going from left to right in Figs. 2–5, we notice that up to $r=R$ all curves collapse as in this range we only probe an ensemble of isolated spheres (note that the spheres have a hardcore radius of R which keeps them from overlap in the Brownian dynamics simulation). The values of W_ν are hence given by Eq. (3). At $r=R$, the volume fraction

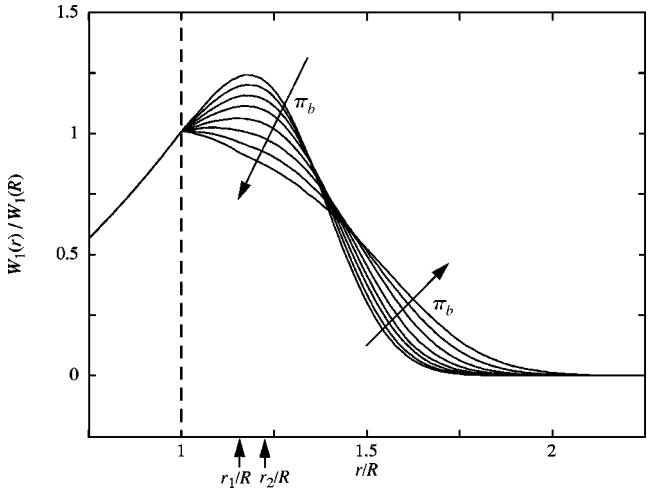

FIG. 3. Minkowski functional $W_1(r)$: Monitoring the progress of network formation of a sample with $\phi=0.4$ and $\Delta E/k_BT=0.0$.

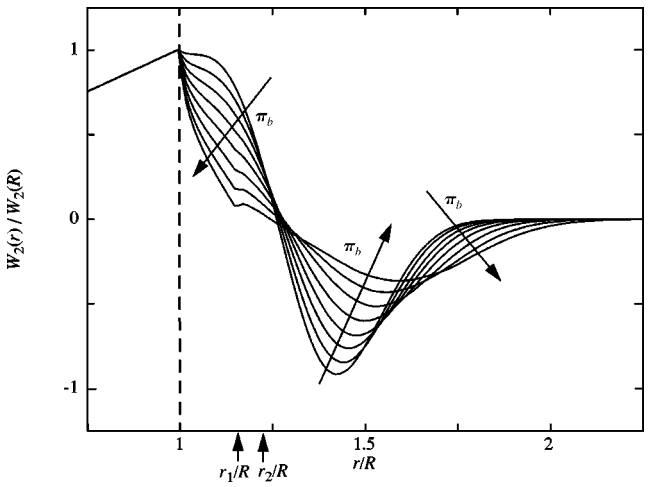

FIG. 4. Minkowski functional $W_2(r)$: Monitoring the progress of network formation of a sample with $\phi=0.4$ and $\Delta E/k_BT=0.0$.

of the real system can be extracted, i.e., $W_0(R)=\phi=0.4$. As the imaginary spheres are blown up beyond $r=R$, many-particle correlation functions come into play, resulting in a separation of the curves for the different values of π_b. The curves come to a constant value when the (overlapping) spheres occupy the entire sample, which results in $W_0=\phi=1$ and $W_1=W_2=W_3=0$. We notice in all four figures that this range becomes broader with progressing network formation, which indicates the existence of larger and larger void spaces. Furthermore, it is interesting that the functions display more characteristics the higher the value of ν. Where the effect of space filling is simply slowed (see Fig. 2), the change in surface shows two regimes for $r>R$. Apart from the extended approach to $W_1(r)=0$, the surface gain [i.e., the slope in $W_1(r)$] just above $r=R$ turns negative which can only occur in the presence of densified regions. How-

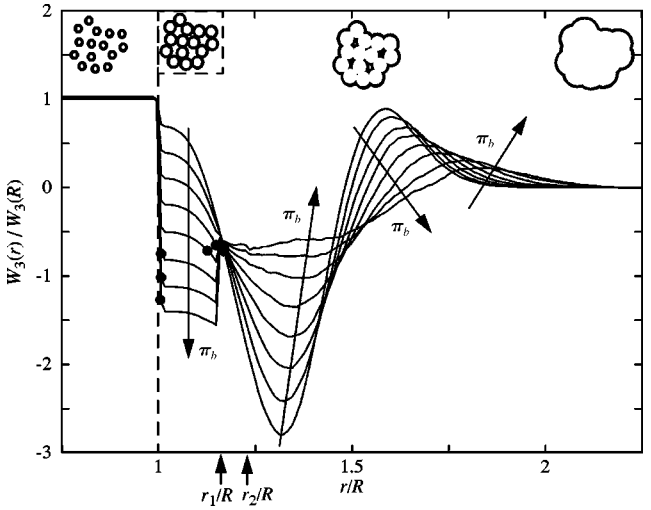

FIG. 5. Minkowski functional $W_3(r)$: Monitoring the progress of network formation of a sample with $\phi=0.4$ and $\Delta E/k_BT=0.0$. The two-dimensional configurations sketch the formation of bonds, cavities, and their destruction as the radius of the imaginary spheres increases.

TABLE III. Critical radius r_c to capture 99% of all particles in a single cluster.

π_b	0.05	0.10	0.15	0.20	0.25	0.30	0.35	0.40
r_c/R	1.167	1.169	1.168	1.154	1.125	1.006	1.004	1.009

ever, the most intriguing function is $W_3(r)$, Fig. 5. Recall that this displays the number of components plus the number of cavities minus the number of tunnels. In order to simplify the discussion, the dots in the figure indicate the r values r_c above which ''almost all'' particles are part of the same cluster (gel), i.e., above which the number of components is close to one. Note that the r dependence of number of components has bad statistics since a few particles situated either in a big void space or close to other particles significantly change the number of components for given r. For that reason, the dots in the figure denote the values above which 99% of all particles are part of the same cluster. The values are also tabulated in Table. III

For interpreting the cavity and tunnel contributions to W_3 contained in Fig. 5, we discuss three characteristic radii, $r=R$, r_1, and r_2. First, tunnels can form as soon as particles may contact. Thus, $r=R$ is a lower limit for the formation of tunnels, i.e., closed loops of particles. Second, considering an equilateral triangle of side length $2R$, one notices that a lower limit for destructing a tunnel is $r_1=2R/\sqrt{3}$ (which is the distance from the center of the triangle to the corners). At the same time, this is also a lower limit for the generation of cavities. Third, considering an equilateral tetrahedron with side length $2R$, the lower limit for the destruction of cavities is $r_2=\sqrt{3/2}R$ (which is the distance from the center of the tetrahedron to its corners). In summary, we expect a strong decrease of $W_3(r)$ at $r=R$ (twofold—decreasing number of components and generation of tunnels), followed by a strong increase above $r_1=2R/\sqrt{3}$ (twofold—destruction of tunnels and generation of cavities), and a weaker decrease above $r_2=\sqrt{3/2}R$ (onefold—destruction of cavities). This should hold with the restriction that distinct changes at r_1 and r_2 can only be seen for the later stages of the network formation, i.e., for higher values of π_b. The change of the connectivity $W_3(r)$ as a function of π_b displayed in Fig. 5 reflects exactly these predictions in the vicinity of $r=R$ and r_1, whereas the (predictively weak) change at r_2 is not observed. We notice that in the interval $[R,r_1]$ the values decrease due to the increased number of bonds between particles. Above r_1 a flattening of the curve is observed, which originates from an increasing degree of heterogeneity: At the beginning of the network formation, the particle distribution is rather homogeneous (compared to the later stages), and the destruction of tunnels and generation of cavities occur in a different r window than the destruction of cavities. In general, the more heterogeneous the structure the more these regimes mix, resulting in a flattening of the connectivity curve by smearing out the extrema. So, in particular, for the connectivity, the fact that the curve turns relatively flat in the range $r>r_1$, in comparison to $r<r_1$, reflects the heterogeneity. This is supported by the approach to the constant value at larger r only. We note that, since the system is in a finite simulation box and boundary effects are not counted, and according to definition (1), $\lim_{R\to\infty}W_3(R)=0$ as there is no surface.

2. Decreasing volume fraction

The effect of developing heterogeneities on the Minkowski functionals has been examined in the preceding section as network formation progresses. We now wish to see the effect of diluting the system. To that end, volume fractions in the range $\phi\in[0.2,0.4]$ in steps of $\Delta\phi=0.025$ have been examined. As the stationary state of the network formation is inaccessible by dynamic computer simulations, the structures examined here correspond to the instant when all clusters/flocs joined to the single cell-spanning network. Although this choice is to a certain degree arbitrary, we point out that the corresponding values of the cross-linking parameter π_b were within 15% of their extrapolated steady state values [29,37,52]. In the present context this is considered to be sufficient as the trends in the results come out clear.

The volume fraction dependence of the Minkowski functionals is shown in Figs. 6–9, where the arrows point in the direction of increasing volume fraction. The trends of the volume fraction dependence are not very clear in the range $[R,r_1]$ for (W_1,W_2,W_3), and the dashed arrow in Fig. 9 indicates the overall trend, which is however not followed by all samples. The influence of change in volume fraction becomes clearer above r_1, where the curves flatten and spread out over a larger region for decreasing volume fraction. Thus, lowering the volume fraction shows similar signs as progressing network formation discussed above, i.e, displays the effects of increasing heterogeneity. The following is noteworthy. While the volume fraction is doubled from the lowest to the highest value, one could argue that the characteristic length scale, over which the heterogeneity extends, decreases by $\sqrt[3]{2}$. Since the characteristic values R, r_1, and r_2 do not change with volume fraction, another natural choice for the characteristic length scale is the r value r_{m}, at which the minimum in $W_2(r)$ in the large r range occurs. The inset in Fig. 8 shows the dependence of this length scale r_{m} on $\phi^{-1/3}$. The lines are drawn to guide the eye. If the increase in the characteristic length scale were only due to the change in volume fraction, the function should be linear. However, the data suggest at least that $r_{\mathrm{m}}(\phi^{-1/3})$ does not follow a single linear law. The length scale grows more than proportional upon increasing $\phi^{-1/3}$, meaning that the change in morphology is not only due to the bulk geometric stretch.

Apart from the larger characteristic length scale, lowering the volume fraction also has the effect of a larger jump in $W_3(r)$ at $r=r_1$, and, in particular, a jump develops at $r=r_2$. Remembering that the values r_1 and r_2 are *lower bounds* for specific, dense structural units, the fact of large jump occur at these values means that more of these close-packed units are present in the low volume fraction samples. This goes in hand with the observation that the large scale structures (voids) are larger than expected only due to solely the stretch $\phi^{-1/3}$, thereby compensating to maintain the prescribed volume fraction.

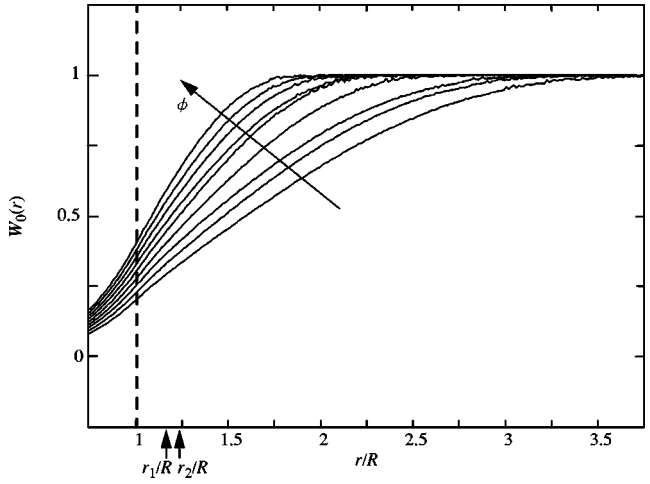

FIG. 6. Minkowski functional $W_0(r)$: Dependence on the volume fraction ϕ for $\Delta E/k_BT=0.0$.

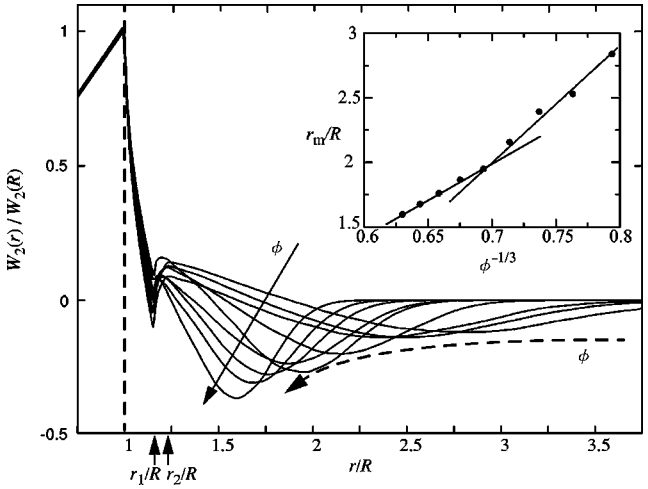

FIG. 8. Minkowski functional $W_2(r)$: Dependence on the volume fraction ϕ for $\Delta E/k_BT=0.0$.

3. Slow versus fast coagulation

The influence of the interaction potential between the particles on the formation of the particle network shall be examined next. This is of interest as in colloidal processing certain structural and/or mechanical properties are desired. Alternation of the particle interaction offers a way to develop appropriate processing routes for obtaining desired structures. We here compare samples at a volume fraction $\phi=0.4$ with interaction potentials having a secondary minimum, as listed in Table II. This interaction potential with varying surface charge shall serve a model to mimic the situation of varying depth of the secondary minimum and energy barrier by changing one parameter. It is this characteristic which is under consideration here, and not the precise form of the interactions in dense colloidal systems.

The secondary minimum in the interaction potential, similar to lowering the volume fraction, results in a coarsening of the morphology, as can be seen from the slower approach of the values $\lim_{r\to\infty}W_\nu(r)$ in Figs. 10–13, in particular, for $\nu=0,1,2$. We notice that in all plots, the curves for $\Delta E/k_BT=0$ are clearly separated form a group of curves to the values $\Delta E/k_BT=0.076,0.522,1.20,2.07$, followed by separate curves for the higher energy barriers. The occurrence of a grouping of the low energy barrier values can be attributed to the fact that in this range the energy barrier is still surmountable by thermal agitation. The curve listed for $\Delta E/k_BT=0$ does not belong to this group. The reason is that it corresponds to a surface potential $\psi_0=0$ mV (pure van der Waals attraction), having a stronger attractive force than the potential for which the energy barrier just vanishes when approaching from $\psi_0=12$ mV. In comparison to the change in volume fraction, the increase in characteristic length scale due to the energy barrier is smaller. However, this is based on the stretch of the curves to larger r values. The identification of a length scale from $W_2(r)$, as done for the volume fraction dependence, manifests a different result. Figure 12 shows that the position of the minimum r_m is approximately constant for $0.0\leqslant\Delta E/k_BT\leqslant3.01$ at $r_m/R\simeq1.6$, slightly decreases for $\Delta E/k_BT=4.31$ to $r_m/R\simeq1.4$ (very flat minimum), and further for $\Delta E/k_BT=5.65$ to $r_m/R=1.23$, as

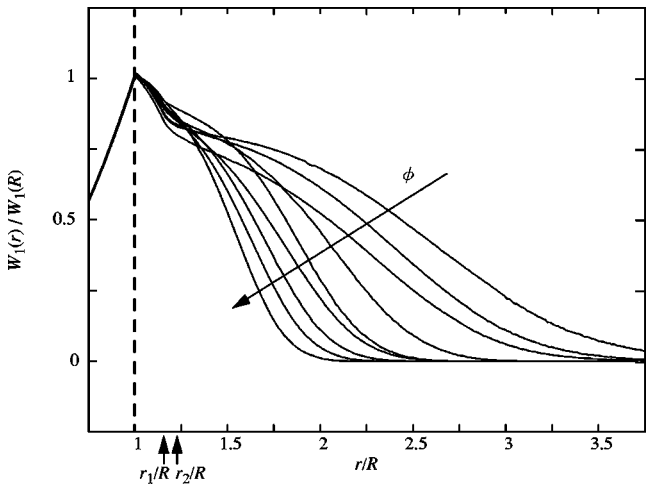

FIG. 7. Minkowski functional $W_1(r)$: Dependence on the volume fraction ϕ for $\Delta E/k_BT=0.0$.

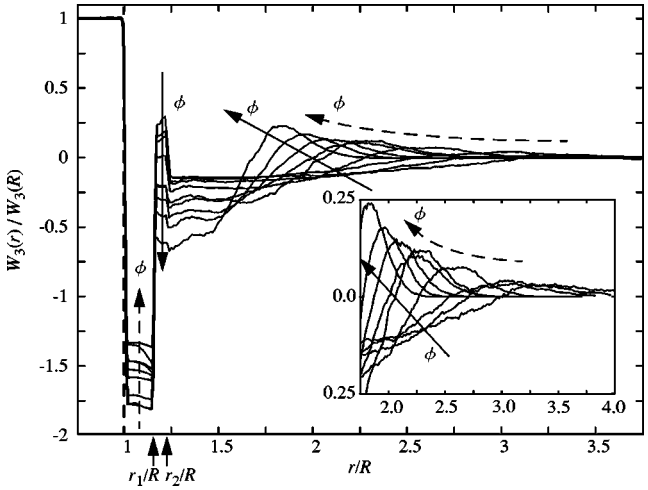

FIG. 9. Minkowski functional $W_3(r)$: Dependence on the volume fraction ϕ for $\Delta E/k_BT=0.0$.

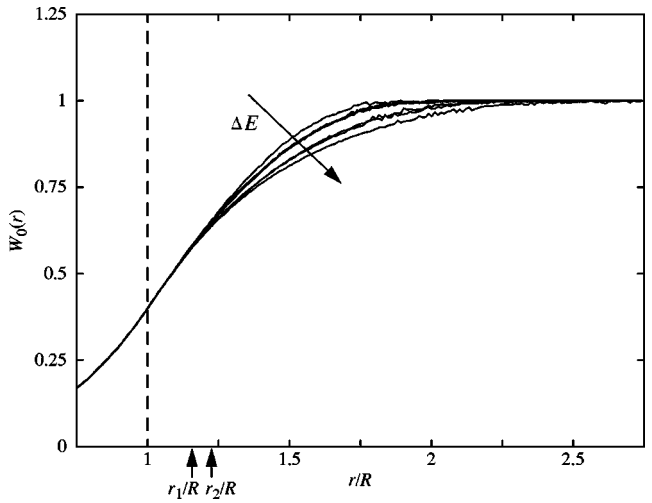

FIG. 10. Minkowski functional $W_0(r)$: Dependence on the energy barrier $\Delta E/k_BT$ at volume fraction $\phi=0.4$.

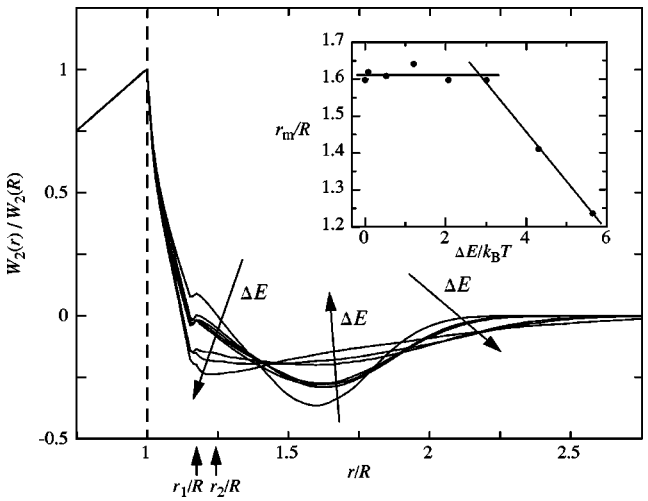

FIG. 12. Minkowski functional $W_2(r)$: Dependence on the energy barrier $\Delta E/k_BT$ at volume fraction $\phi=0.4$.

shown in the inset of Fig. 12 (the lines are drawn to guide the eye). The connectivity (see Fig. 13) flattens above $r_m/R \geqslant 1.4$ due to the energy barrier, reflecting a rather polydisperse distribution of voids. In contrast to the volume fraction influence on the connectivity, the energy barrier does not lead to the sharp jumps at $r=r_1$ and r_2. In summary, the energy barrier increases the heterogeneity of the network, however, equilateral tetrahedra are not as significant building blocks of the structure as for the low volume fractions. Finally, we note that in the range $[R,r_1]$ the curves show a stronger decrease than in the absence of an energy barrier. This can be attributed to particles captured in the secondary energy minimum, which is localed approximately in the middle of this interval for all barriers examined here.

D. Comparison to other structural analyses

The structural analysis of colloidal particle gels generated from dynamic computer simulations most often concentrate on the pair-correlation function. It has been revealed that fast coagulation at high volume fractions results in a freezing of the liquid structure, whereas lower volume fractions and/or a secondary minimum in the particle interaction allow substantially more particle rearrangements and change in morphology [26,25,32]. This is in agreement with the results presented here. However, the information contained in these two techniques of structure analysis are not identical and in the author's opinion both methods have their own right. The Minkowski analysis includes *n*-point distribution functions for $n>2$ and allows to discuss the heterogeneity as illustrated above, but it is limited to analyze the structure on length scales smaller than the radius of the largest void [above which the functions $W_\nu(r)$ remain constant]. This restriction clearly does not apply to the pair correlation function. The latter allows, e.g., to analyze the freezing of the liquid structure on a wide range of length scales in fast coagulation.

A decrease in the volume fraction does not simply translate inversely proportionally into a larger characteristic size

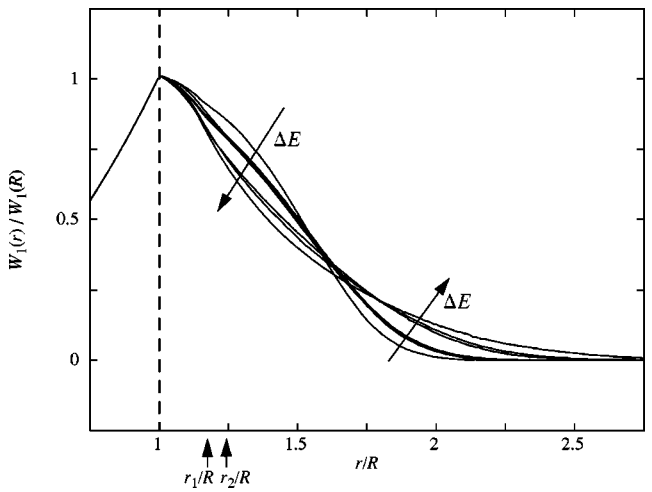

FIG. 11. Minkowski functional $W_1(r)$: Dependence on the energy barrier $\Delta E/k_BT$ at volume fraction $\phi=0.4$.

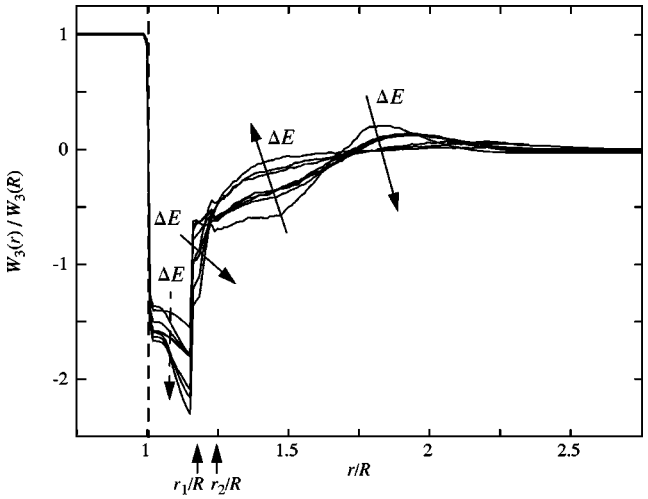

FIG. 13. Minkowski functional $W_3(r)$: Dependence on the energy barrier $\Delta E/k_BT$ at volume fraction $\phi=0.4$.

of void spaces, but rather increases the degree of heterogeneity even more as shown above. This corresponds to the results found using Voronoi analysis (see, e.g., Refs. [24,53]), which examines the statistical distribution of Voronoi cell volumes in a given configuration. Using confocal laser scanning microscopy to determine the local spatial structures in dense colloidal gels, ''surprisingly long tails'' were found in that distribution as the volume fraction is lowered [24], indicating a large degree of heterogeneity. In general, the Voronoi analysis relates closest to the Minkowski functional $W_1(r)$ of the four available, thus to the pore size distribution given by Eq. (5). They both probe the amount of free space around particles, whereas the other three Minkowski functionals provide then additional information.

The pore structure has been analyzed by a measure closely related to $W_1(r)$ on simulated gels [30,31]. It was found that the presence of an attractive nonbonding interaction on long length scales enhances the formation of larger pores. This may be due to an energetic preference for rather dense regions, with accordingly big pores. In the present study, the interaction potential also exhibits a shallow secondary energy minimum for $\psi_0 \geqslant 12$ mV at intermediate distances, in addition to an energy barrier. The latter results in a larger diffusion in phase space before primary, irreversible bonds are formed. Thus, the simulations results indicate that a (shallow) long range attraction in combination with the higher capability for configurational rearrangements prior to bond formation favor a higher heterogeneity.

The local building blocks of the particle network have been examined in detail in terms of the bond-angle distribution function and of the so-called ''triangle''-distribution function [32], measuring the areas of trihedra spanned by bond-connector vectors starting from the same center particle. The combined analysis allowed to determine, among other building blocks, the frequency of equilateral triangles and equilateral tetrahedra. These are strongly enhanced in the low volume fraction samples [32], in accordance with the findings from Fig. 9 in this study.

IV. CONCLUSIONS

The structure of colloidal particle networks generated by Brownian dynamics simulations was analyzed in terms of the Minkowski functionals of integral geometry, using the parallel-body technique. The analysis revealed that decreasing the volume fraction and/or the presence of an energy barrier allow for larger heterogeneity to develop. It has been found that the use of all four Minkowski functionals, instead of solely the pore size distribution used elsewhere, indeed reveals further interesting details, in particular, the average mean curvature $W_2(r)$ and the connectivity $W_3(r)$.

The Minkowski functionals are, in the author's view, another useful tool for structural analysis in addition to the commonly used pair-correlation function and bond-angle distribution function. The difference between them being, first, the different length scales at which structural features are resolved and second, the dependence on higher order distribution functions. As shown in the discussion of the results, these methods of analysis overlap in certain regimes, thereby strengthening each method on its own. Thus, it rather depends on the specific interest in the structure, which of the measures shall be used. Studying the freezing of the liquid structure upon fast coagulation at high volume fractions, the pair-correlation function is a useful measure. If the interest focuses on the analysis of the heterogeneity of the network, the method of choice could be the Minkowski functionals as elaborated in this study.

The precise definition of a pore size distribution, or simply of a pore, has not been attempted here. Although the present analysis allows to talk about heterogeneities and examine their extent, the way of how to measure void space and pores is still unclear. The connectivity $W_3(A_r;\{\rho_n\})$ as a function of r, however, may serve as a measure even of practical significance for describing the macroscopic permeability of a network.

The use of Minkowski functionals with the parallel- body technique is not restricted to computer simulations. The ability of confocal laser scanning microscopy to determine particles' 3D coordinates to high precision allows to postprocess the data with the technique described here in order to obtain new and exciting insight into the structure of the network.

ACKNOWLEDGMENTS

The author thanks Dr. Thomas Buchert and Dr. Jens Schmalzing for providing the code to evaluate the Minkowski functionals and for their helpful advice.

[1] D.A. Weitz and M. Oliveria, Phys. Rev. Lett. **52**, 1433 (1984).
[2] D.A. Weitz, J.S. Huang, M.Y. Lin, and J. Sung, Phys. Rev. Lett. **54**, 1416 (1985).
[3] D.A. Weitz and Y. Lin, Phys. Rev. Lett. **57**, 2037 (1986).
[4] C. Cametti, P. Codastefano, and P. Tartaglia, Phys. Rev. A **36**, 4916 (1987).
[5] J.L. Burns, Y. Yan, G.J. Jameson, and S. Biggs, Langmuir **13**, 6413 (1997).
[6] E. Overbeck, C. Sinn, T. Palberg, and K. Schatzel, Colloids Surf., A **122**, 83 (1997).
[7] L.B. Aberle *et al.*, Appl. Opt. **37**, 6511 (1998).
[8] C. Urban and P. Schurtenberger, J. Colloid Interface Sci. **207**, 150 (1998).
[9] A. Moussaïd and P.N. Pusey, Phys. Rev. E **60**, 5670 (1999).
[10] P. Poulin, J. Bibette, and D.A. Weitz, Eur. Phys. J. B **7**, 277 (1999).
[11] S. Romer *et al.*, Philos. Trans. R. Soc. London, Ser. A **359**, 977 (2001).
[12] J.S. Reed, *Principles of Ceramics Processing* (Wiley, New York, 1996).
[13] R. Hilfer, in *Advances in Chemical Physics*, edited by I. Prigogine and S.A. Rice (Wiley, New York, 1996), Vol. XCII.

[14] R. Menold, B. Lüttge, and W. Kaiser, Adv. Colloid Interface Sci. **5**, 281 (1976).
[15] C.C. Donaldson, J. McMahon, R.F. Stewart, and D. Sutton, Colloids Surf. **18**, 373 (1986), and references therein.
[16] H. von Both, R. Oberacker, and M.J. Hoffmann, Z. Metallkd. **90**, 996 (1999).
[17] L. Bachmann and E. Mayer, in *Cryotechniques in Biological Electron Microscopy*, edited by R.A. Steinbrecht and K. Zierold (Springer, Berlin, 1987), p. 3.
[18] H. Moor, in *Cryotechniques in Biological Electron Microscopy*, edited by R.A. Steinbrecht and K. Zierold (Springer, Berlin, 1987), p. 175.
[19] H.M. Wyss *et al.*, J. Colloid Interface Sci. **248**, 340 (2002).
[20] P. Cornillon, M.J. McCarthy, and D.S. Reid, J. Texture Stud. **28**, 421 (1997).
[21] A. van Blaaderen and P. Wiltzius, Science **270**, 1177 (1995).
[22] E.R. Weeks *et al.*, Science **287**, 627 (2000).
[23] A.B. Dinsmore and D.A. Weitz, J. Phys.: Condens. Matter **14**, 7581 (2002).
[24] P. Varadan and M.J. Solomon, Langmuir **19**, 509 (2003).
[25] G.C. Ansell and E. Dickinson, Faraday Discuss. **83**, 167 (1987).
[26] E. Dickinson, J. Colloid Interface Sci. **118**, 286 (1987).
[27] B.H. Bijsterbosch *et al.*, Faraday Discuss. **101**, 51 (1995).
[28] M.T.A. Bos and J.H.J. van Opheusden, Phys. Rev. E **53**, 5044 (1996).
[29] M. Whittle and E. Dickinson, Mol. Phys. **90**, 739 (1997).
[30] M. Whittle and E. Dickinson, Mol. Phys. **96**, 259 (1999).
[31] E. Dickinson, J. Colloid Interface Sci. **225**, 2 (2000).
[32] M. Hütter, J. Colloid Interface Sci. **231**, 337 (2000).
[33] C. Thornton and D.J. Barnes, Acta Mech. **64**, 45 (1986).
[34] C.-h. Lui *et al.*, Science **269**, 513 (1995).
[35] S.N. Coppersmith *et al.*, Phys. Rev. E **53**, 4673 (1996).
[36] G.W. Baxter, in *Proceedings of the International Conference on Powders and Grains 97, Durham, North Carolina, 1997*, edited by R.P. Behringer and J.T. Jenkins (Balkema, Rotterdam, 1997), p. 345.
[37] M. Hütter, Phys. Chem. Chem. Phys. **1**, 4429 (1999).
[38] H. Hadwiger, *Vorlesungen über Inhalt, Oberfläche und Isoperimetrie* (Springer, Heidelberg, 1957).
[39] L.A. Santalò, *Integral Geometry and Geometric Probability* (Addison-Wesley, Reading, MA, 1976).
[40] R. Schneider, *Convex Bodies: The Brunn-Minkowski Theory* (Cambridge University Press, Cambridge, 1993).
[41] W. Weil, in *Convexity and Its Applications*, edited by P.M. Gruber and J.M. Wills (Birkhäuser, Basel, 1983).
[42] K.R. Mecke, in *Statistical Physics and Spatial Statistics: The Art of Analyzing and Modeling Spatial Structures and Pattern Formation*, edited by K.R. Mecke and D. Stoyan (Springer, Berlin, 2000).
[43] K.R. Mecke, T. Buchert, and H. Wagner, Astron. Astrophys. **288**, 697 (1994).
[44] M. Kerscher *et al.*, Astron. Astrophys. **377**, 1 (2001).
[45] S. Torquato, B. Lu, and J. Rubinstein, Phys. Rev. A **41**, 2059 (1990).
[46] S. Torquato and M. Avellaneda, J. Chem. Phys. **95**, 6477 (1991).
[47] B. Lu and S. Torquato, J. Chem. Phys. **98**, 6472 (1993).
[48] R. Kubo, M. Toda, and N. Hashitsume, *Statistical Physics II: Nonequilibrium Statistical Mechanics*, 2nd ed. (Springer, Berlin, 1991).
[49] H.C. Öttinger, *Stochastic Processes in Polymeric Fluids. Tools and Examples for Developing Simulation Algorithms* (Springer, Berlin, 1996).
[50] P.E. Kloeden and E. Platen, *Numerical Solution of Stochastic Differential Equations* (Springer, Berlin, 1992).
[51] K.R. Mecke and H. Wagner, J. Stat. Phys. **64**, 843 (1991).
[52] M. Hütter, Ph.D. thesis, ETH, Zürich, Switzerland, 1999. http://e-collection.ethbib.ethz.ch/show?type=diss&nr=13107
[53] F.W. Starr, S. Sastry, J.F. Douglas, and S.C. Glotzer, Phys. Rev. Lett. **89**, 125501 (2002).